

ViTMAlis: Towards Latency-Critical Mobile Video Analytics with Vision Transformers

Miao Zhang, *Member, IEEE*, Guanzhen Wu, Hao Fang, Yifei Zhu, *Member, IEEE*, Fangxin Wang, *Member, IEEE*, Ruixiao Zhang, and Jiangchuan Liu, *Fellow, IEEE*,

Abstract—Edge-assisted mobile video analytics (MVA) applications are increasingly shifting from using vision models based on convolutional neural networks (CNNs) to those built on vision transformers (ViTs) to leverage their superior global context modeling and generalization capabilities. However, deploying these advanced models in latency-critical MVA scenarios presents significant challenges. Unlike traditional CNN-based offloading paradigms where network transmission is the primary bottleneck, ViT-based systems are constrained by substantial inference delays, particularly for dense prediction tasks where the need for high-resolution inputs exacerbates the inherent quadratic computational complexity of ViTs. To address these challenges, we propose a dynamic mixed-resolution inference strategy tailored for ViT-backboned dense prediction models, enabling flexible runtime trade-offs between speed and accuracy. Building on this, we introduce ViTMAlis, a ViT-native device-to-edge offloading framework that dynamically adapts to network conditions and video content to jointly reduce transmission and inference delays. We implement a fully functional prototype of ViTMAlis on commodity mobile and edge devices. Extensive experiments demonstrate that, compared to state-of-the-art accuracy-centric, content-aware, and latency-adaptive baselines, ViTMAlis significantly reduces end-to-end offloading latency while improving user-perceived rendering accuracy, providing a practical foundation for next-generation mobile intelligence.

Index Terms—Vision transformers, Mobile video analytics, Resource management

I. INTRODUCTION

THE rapid proliferation of mobile computing platforms and edge infrastructure has fueled a surge in mobile video analytics (MVA) applications, ranging from augmented reality (AR) to autonomous mobile sensing [1]–[3]. These applications rely heavily on advanced computer vision models to deliver real-time, interactive user experiences. While existing MVA systems have predominantly been built on convolutional neural networks (CNNs), their long-standing dominance has been increasingly challenged by vision transformers (ViTs) [4], a family of backbones derived from the Transformer architecture [5]. With improved global context modeling and reduced inductive bias, ViTs have achieved state-of-the-art performance across various vision tasks [6]–[8]. Their ability to handle flexible input sizes and generalize across tasks and modalities has established them as foundational vision models

Miao Zhang, Guanzhen Wu, Hao Fang, and Jiangchuan Liu are with the School of Computing Science, Simon Fraser University, Canada. Yifei Zhu is with Global College, Shanghai Jiao Tong University, China. Fangxin Wang is with School of Science and Engineering (SSE) and The Future Network of Intelligence Institute (FNii), The Chinese University of Hong Kong, Shenzhen, China. Ruixiao Zhang is with Computer Science Department, University of Illinois Urbana-Champaign, United States.

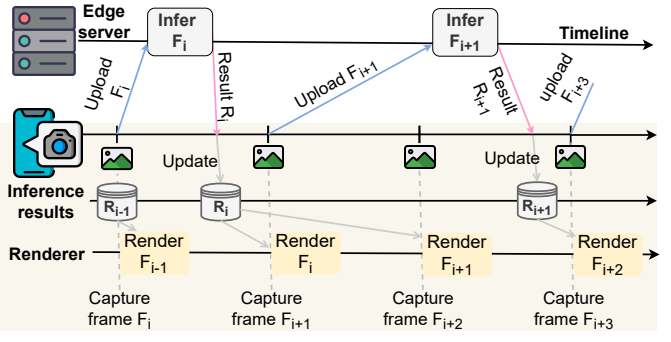


Fig. 1. Edge-assisted mobile video analytics.

[9], [10]. In particular, ViTs now serve as image or video encoders in vision foundation models [10], [11] and vision-language models [12], [13], providing the core intelligence for next-generation mobile applications.

However, integrating ViTs into latency-critical MVA applications faces significant challenges. Unlike general video analytics tasks that can tolerate processing delays ranging from several seconds to minutes [14]–[16], MVA applications often involve real-time user interaction and are thus highly sensitive to latency. As illustrated in Fig. 1, the prevailing *edge-assisted paradigm* of MVA [1] typically involves offloading video frames captured by a mobile device to an edge server for inference, with the results returned to the mobile device for on-device rendering (e.g., overlaying bounding boxes or labels onto objects appearing in the live camera view). This offloading process forms a *real-time feedback loop* that is intrinsic to interactive MVA. Even minor additional delays introduced in the loop can cause stale outputs that lag behind the user’s live view, resulting in degraded visual experiences.

Given the stringent latency requirements of MVA, previous work has largely concentrated on minimizing the end-to-end (E2E) offloading latency through system-level optimizations. Since these systems predominantly rely on CNN-backboned models, which are relatively lightweight compared to their ViT counterparts, they typically assume that server-side inference delay is relatively constant and not the dominant contributor to the E2E offloading latency [1], [17], [18]. Thus, their optimization efforts focus mainly on reducing the delays incurred by transmitting video data over mobile networks. Nevertheless, this assumption no longer holds for ViT-backboned models, where the model inference emerges as the dominant bottleneck.

Vision tasks performed in MVA are principally *dense pre-*

diction tasks (e.g., object detection and semantic segmentation), which typically require high-resolution input images to maintain accuracy [18]. However, the multi-head attention mechanism in ViT introduces inference time and memory complexity that scale quadratically with the number of input tokens (and thus with image resolution). Even with architectural optimizations such as window attention [7], inference delay remains significant. For instance, our measurements show that a ViT-backboned dense prediction model, *ViTDet-L* [7], incurs an inference delay of approximately 281 ms when processing a 1080p frame on an edge server equipped with an NVIDIA RTX 5090 GPU, which corresponds to only 3.56 frames per second (FPS).

To reduce the inference delay, various inference-time acceleration techniques have been explored to balance inference speed and accuracy by leveraging the input-agnostic nature of ViTs [19]. While pruning or merging less informative vision tokens in intermediate ViT layers has shown effectiveness in tasks such as image and video classification [20]–[22], these methods often incur irreversible visual detail loss, which can significantly degrade the accuracy of dense prediction tasks. Mixed-resolution tokenization techniques [23], [24], which accelerate inference by allowing each token to represent image regions of varying sizes, have emerged as promising alternatives. However, their potential for dense prediction tasks remains largely unexplored.

To bridge the gap between ViT-backboned vision models and MVA, we explore, for the first time, system-level design opportunities that leverage the unique characteristics of ViTs to address their practical deployment challenges. We tailor our designs to dynamic mobile network conditions and diverse video content to enable the efficient deployment of ViT-backboned vision models in MVA scenarios. Specifically, we present ViTMAlis, a ViT-native offloading system that optimizes resource efficiency for edge-assisted MVA. At its core, ViTMAlis incorporates a mixed-resolution compression and inference strategy, specifically designed for ViTs, to jointly reduce network transmission and server-side inference delays. Our contributions can be summarized as follows:

- We propose a *dynamic mixed-resolution inference* strategy for ViT-backboned dense prediction models. It employs a carefully designed region partitioning method to produce mixed-resolution vision tokens that can be seamlessly processed by pre-trained ViT backbones. To maintain compatibility with dense prediction heads requiring full-resolution features, it further includes a feature reconstruction mechanism that dynamically restores the full-resolution feature map from mixed-resolution tokens, enabling flexible trade-offs between model inference speed and accuracy.
- We develop ViTMAlis, a ViT-native MVA system that incorporates our mixed-resolution inference strategy and dynamically adapts configuration for each offloaded frame based on network conditions and video content. By combining an *accuracy-oriented downsampling region selection* method with *content-aware performance estimation*, ViTMAlis optimizes the E2E offloading latency and rendering accuracy from a system-wide perspective.

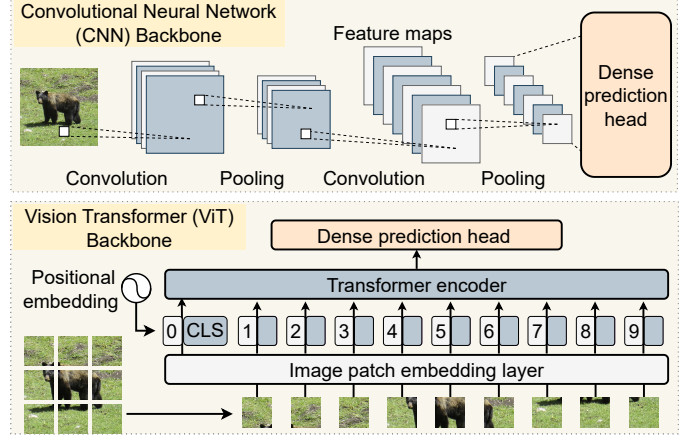


Fig. 2. CNNs and ViTs employ different strategies to extract visual features from images.

- We implement and deploy a fully functional prototype of ViTMAlis on commodity mobile and edge devices. The implementation confirms the practical feasibility of the proposed system, showing that it can be seamlessly integrated into today's mobile computing platforms.
- We conduct extensive experiments using videos captured in diverse mobile scenarios and evaluate the system under varying mobile network conditions. The results demonstrate that, compared to existing accuracy-centric, content-aware, and latency-adaptive baselines, ViTMAlis significantly reduces E2E offloading latency while improving user-perceived rendering accuracy, validating its effectiveness for latency-critical MVA.

II. BACKGROUND AND MOTIVATION

MVA involves applying computer vision models to analyze the video captured by mobile devices' cameras in real time [2], [17], [18], [25]. Due to the limited computational resources and heat dissipation constraints of mobile devices, it is impractical to execute accurate yet resource-intensive models locally for real-time inference. The edge-assisted MVA paradigm addresses this challenge by offloading video frames from mobile devices to edge servers for inference. In this context, both the quality (i.e., remote inference accuracy) and the freshness of the returned inference results are critical. As illustrated in Fig. 1, the freshness of an offloaded frame is determined by its E2E offloading latency, which comprises the frame encoding and upload delays, the server-side decoding and inference delays, and the negligible result download delay. Existing edge-assisted solutions primarily utilize relatively lightweight CNN-backboned models, typically assuming a fixed model inference delay and thus focusing on frame compression strategies to balance network transmission delay against inference accuracy [1], [2], [17]. Nonetheless, when ViT-backboned models are employed, optimizing solely for network transmission delay becomes suboptimal.

ViT as a General-Purpose Backbone. As Fig. 2 illustrates, when serving as backbones for general visual feature extraction, vanilla ViTs split the input image into *fixed-size* (e.g.,

16×16 pixels), non-overlapping image patches, linearly embed each of them, add positional embeddings, and then feed the resulting sequence of embeddings into a Transformer encoder [4]. Unlike CNNs, vanilla ViTs maintain a *single-scale* feature map throughout the network, capturing global dependencies and long-range relationships across the entire image.

Dense prediction tasks in MVA, such as object detection and instance segmentation, require a fine-grained understanding of object instances across multiple scales and therefore necessitate *high-resolution* input images. This contrasts with image or video classification tasks, which operate effectively at lower resolutions (e.g., 224×224) [26], [27]. Unfortunately, the self-attention mechanism in the Transformer encoder of ViTs exhibits computational complexity that scales quadratically with the input sequence length, severely limiting their scalability to high-resolution inputs [24]. For example, increasing the input image resolution from 360p to 1080p increases the inference delay of ViTDet-L by $7.2 \times$ (from 39 ms to 281 ms). These observations highlight the need for specialized system designs to mitigate the substantial inference delay incurred by ViT-backboned models in dense prediction tasks.

Inference-Time Acceleration for ViTs. In ViTs, embedded image patches are processed in a manner analogous to tokens in natural language processing (NLP). The self-attention mechanism theoretically supports input token sequences of arbitrary lengths. Therefore, pre-trained ViT models can naturally handle images of varying resolutions, provided that positional embeddings are scaled appropriately [4]. This input-agnostic property creates unique opportunities to balance runtime inference speed and accuracy by dynamically adjusting token count and arrangement during inference.

One prevalent approach prunes or merges less informative tokens in the intermediate layers of ViT backbones [21], [28]–[30], reducing computation by removing tokens entirely or combining similar ones. Alternative approaches explore performing token reduction during the image preprocessing stage by replacing the uniform grid-based tokenization of vanilla ViTs with mixed-resolution tokenization [23], [24]. They allocate more tokens to important image regions and fewer to less important ones, preserving complete coverage while making more efficient use of a limited token budget [24].

Although promising, most existing acceleration techniques are developed for image and video classification tasks, where a classification head is attached directly to the [CLS] token. In such cases, vision tokens are aggregated into a single global representation via the [CLS] token for image-level or video-level prediction, rendering the precise spatial arrangement of tokens less important. In comparison, dense prediction heads require multi-scale feature maps (i.e., a feature pyramid) from the backbone to handle objects at varying scales effectively. These feature maps are typically constructed on regular 2D grids to preserve spatial alignment, which is essential for downstream prediction heads that operate on grid-aligned and multi-scale features. However, token pruning removes tokens entirely, breaking the uniform spatial coverage, while token merging and mixed-resolution tokenization change token granularity by producing tokens that represent image regions of varying sizes. All of these disrupt the regular grid layout,

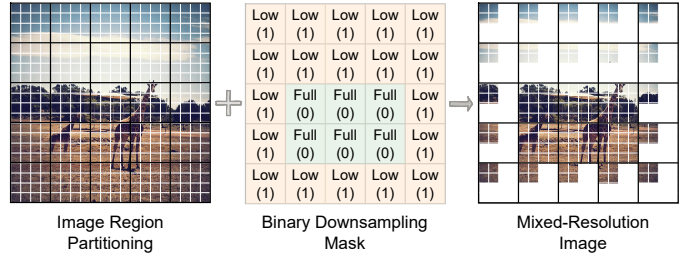


Fig. 3. Inference-compatible region partitioning.

complicating their integration with dense prediction heads.

III. DYNAMIC MIXED-RESOLUTION INFERENCE

To overcome the aforementioned challenges, we introduce a *dynamic mixed-resolution inference strategy* tailored for dense prediction models. We prioritize mixed-resolution tokenization over pruning or merging alternatives, as it enables early-stage computational savings while requiring no architectural modifications or retraining of the pre-trained ViT backbones. The following subsections detail the key designs that address the unique challenges of extending mixed-resolution inference to dense prediction models.

A. Inference-Compatible Region Partitioning

The first challenge is choosing the spatial extent of the image region represented by each token. In standard pre-trained ViT backbones, each token corresponds to a fixed-size image patch, typically 16×16 pixels [4]. To maintain compatibility with pre-trained models, the dimensions of downsampled regions must be integer multiples of the expected patch size. Furthermore, ViT variants designed for dense prediction tasks often replace global attention with window attention in intermediate Transformer blocks to improve efficiency when handling high-resolution inputs [7], [31]. Window attention divides the input feature map into non-overlapping local windows and restricts self-attention computations within each window. To preserve structural consistency under this mechanism, downsampled regions must maintain spatial alignment and consistent patch granularity within each window.

To address this issue, we propose an *inference-compatible region partitioning* method that aligns with the patchification and window attention mechanisms of pre-trained ViT backbones. An illustrative example is shown in Fig. 3, where a coarse-grained grid (shown in black) is overlaid on the image. Each black grid cell, termed a *decision region*, spans $r \times r$ image patches, with each patch (shown in white) being 16×16 pixels. Downsampling decisions are made at the decision region level, producing a binary region-level downsampling mask. The regions marked as low resolution are then downsampled by a factor of d , reducing the number of image patches (and thus tokens) required to represent these regions by a factor of d^2 . To ensure compatibility with the ViT backbone's window attention computation, r is strategically set to $w \times d$, where w is the window size used by the ViT backbone to calculate window attention. In the example shown, both

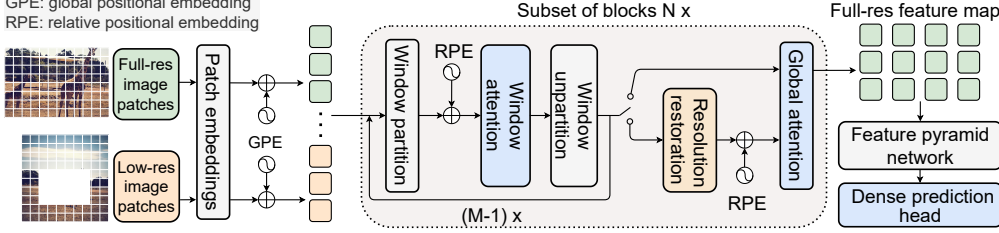


Fig. 4. An example of how dynamic mixed-resolution inference works for ViTDet.

w and d are set to 2, yielding $r = 4$. This choice ensures that tokens from downsampled regions fit exactly within each 2×2 window, allowing the mixed-resolution sequence to be partitioned into windows and reconstructed seamlessly without structural mismatch.

B. Flexible Resolution Restoration

Although a recent study [7] has shown the feasibility of constructing a feature pyramid from the single-scale feature map produced by vanilla ViT backbones, the introduction of mixed-resolution tokenization disrupts this regular spatial layout by producing tokens at varying granularities. As Fig. 3 shows, the original 2D spatial relationships among the image patches are no longer preserved after downsampling. Consequently, additional mechanisms are needed to restore spatial alignment and enable the construction of coherent feature maps required by dense prediction heads.

To address this challenge, we propose a flexible feature map construction method that selectively restores the resolution of tokens corresponding to downsampled image regions at configurable stages within the ViT backbone. This design enables the reconstruction of spatially structured feature maps required by dense prediction heads, while preserving computational efficiency. Fig. 4 illustrates how this method integrates with ViTDet. In ViTDet, the pre-trained ViT backbone is evenly divided into N subsets (default $N = 4$), each containing M Transformer blocks. Within each subset, the first $(M - 1)$ blocks compute local window attention to reduce computational overhead, while the last block applies global attention to enable cross-window information propagation.

Unless otherwise specified, we use the pre-trained ViTDet-L [32] model from the ViTDet family throughout this paper, with $M = 6$ blocks per subset. Unlike the original ViTDet-L, which processes a uniform grid of image patches, our approach separately projects low-resolution and full-resolution image patches into token embeddings. Global positional embeddings are then added to both sets of tokens before they are concatenated and processed by the Transformer blocks. In principle, the full-resolution feature map can be constructed by upsampling low-resolution tokens at any depth within the ViT backbone. However, we find that within each subset, performing restoration between the last window attention block and the subsequent global attention block offers the best trade-off between accuracy and inference delay. We therefore designate this position as the candidate *restoration point* (*RP*) for each subset.

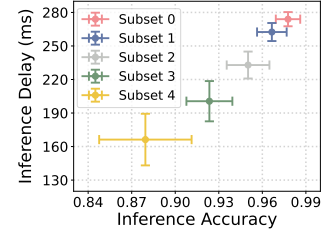


Fig. 5. Impacts of RPs.

Fig. 5 presents the trade-off when restoration is applied at the candidate RPs across different subsets. In this pilot experiment, decision regions that do not contain objects are downsampled by a factor of 2. “Subset 0” represents a special case in which downsampled image patches are first upsampled to full resolution before being fed into the backbone. As shown, applying restoration earlier in the backbone leads to higher accuracy but yields smaller reductions in inference delay. Importantly, our mixed-resolution inference strategy is an *input-adaptive* scheme that dynamically adjusts the input tensor shape for each Transformer block. It preserves the ViT backbone architecture and introduces no additional trainable parameters, thereby enabling seamless integration with any pre-trained ViT backbone.

IV. ViT-NATIVE MVA OFFLOADING FRAMEWORK

A. Joint Network and Inference Optimization

Network transmission delay and server-side vision model inference delay are the primary contributors to the E2E offloading latency in MVA. *Network-centric* efforts treat the model inference delay as constant and focus on reducing the former through various frame compression techniques. For instance, region-of-interest (RoI)-based mixed-quality compression reduces bandwidth by applying higher quality (e.g., lower quantization parameters) to RoIs while aggressively compressing background regions [17]. However, these methods only address transmission delay. Once frames arrive at the server, they are typically decoded to a uniform resolution before processing, leaving inference costs unchanged. Conversely, *inference-centric* efforts often overlook network transmission challenges, assuming input images are already available on the server. While they employ techniques such as mixed-resolution tokenization to accelerate server-side inference [23], [24], these solutions are generally designed for independent images, missing the opportunity to exploit temporal locality across consecutive video frames for more informed optimization.

Achieving simultaneous reduction of network transmission and model inference delays is challenging with existing offloading frameworks and often incurs significant accuracy loss. This is primarily because these frameworks rely on CNN-backboned vision models, which require input images of uniform resolution to preserve spatial relationships within the generated feature maps. Consequently, existing methods often resort to transmitting frames at a uniformly downsampled resolution [2], [25], causing considerable accuracy degradation due to the loss of fine-grained details in important

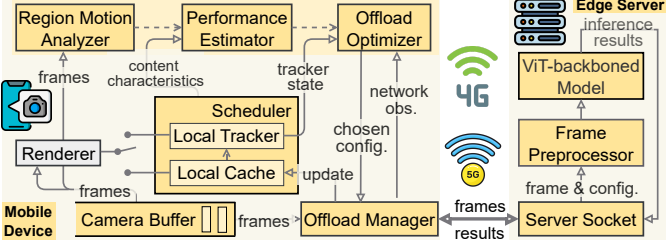


Fig. 6. System overview of ViTMALis.

image regions. In contrast, the architectural flexibility of ViT-backboned models relaxes this uniform-resolution constraint, effectively opening new avenues for joint network and inference optimization.

To fully leverage this potential, we argue that the assignment of region-specific resolutions should not be deferred to the server. Instead, this decision process should originate on the mobile device during the offloading preparation stage. By downsampling less informative regions prior to transmission, we can simultaneously reduce network bandwidth consumption and server-side computational load, thereby cutting latency in both stages. To preserve inference accuracy, the device must estimate the relevance of each region with respect to the server-side inference task and assign resolutions accordingly.

B. System Overview

We first present an overview of ViTMALis, a ViT-native MVA offloading system built upon our proposed mixed-resolution inference strategy. As shown in Fig. 6, ViTMALis follows the canonical edge-assisted MVA paradigm. The mobile device camera continuously captures video frames at a fixed rate and stores them in a *Camera Buffer*. The *Renderer* polls the *Scheduler* at the same rate to retrieve the analytics result corresponding to the frame to be rendered. In edge-assisted MVA, maintaining real-time offloading speed remains a challenge given the scarcity and dynamic nature of mobile network bandwidth. When the E2E offloading latency of a frame exceeds the interval between two consecutive frames (e.g., 33 ms for 30 FPS video), newly captured frames must rely on stale inference results from previously offloaded frames for rendering. To mitigate this issue, lightweight on-device trackers are commonly employed to propagate these stale results to subsequent frames, reducing accuracy degradation when up-to-date remote inference results are unavailable [2], [17], [25].

The *Scheduler* in ViTMALis consists of two key components: a *Local Cache* that stores the remote inference result of the most recently offloaded frame and a *Local Tracker* that uses lightweight tracking techniques to generate up-to-date results for newly captured frames. When a frame is queried, the *Scheduler* first checks the *Local Cache*. If the cached remote inference result corresponds to the queried frame, it is returned. Otherwise, the result from the *Local Tracker* is used. Upon receiving new remote inference results, the *Offload Manager* updates the *Local Cache*. This update triggers both the reinitialization of the *Local Tracker* to synchronize with

the latest result and the scheduling of the subsequent frame for offloading.

For each frame to be offloaded, we define a *configuration* $c \in \mathcal{C}$ as $c = (\tau_d, \lambda, \beta)$, where \mathcal{C} is the set of all candidate configurations. Here, τ_d determines the downsampling mask for decision regions, λ denotes the compression quality parameter for the mixed-resolution frame, and β specifies the restoration point within the ViT backbone for mixed-resolution inference.

The frame offloading workflow operates as follows. The *Region Motion Analyzer* first computes motion values for each decision region and forwards them to the *Performance Estimator*. This estimator integrates the motion values with regional content characteristics from the *Local Tracker* to predict the compressed data size and expected inference accuracy for each candidate configuration. Finally, the *Offload Optimizer* leverages these predictions, alongside recent network observations and the current tracker state, to select the optimal offloading configuration, denoted as c^* .

Once c^* is chosen, the *Offload Manager* generates a binary downsampling mask based on τ_d^* . This mask is used to produce a single mixed-resolution image (as shown in Fig. 3), which is then compressed using the quality parameter λ^* . The compressed frame and its configuration are transmitted to the server. Upon receipt, the server extracts the low- and full-resolution patches based on the downsampling mask, constructs the mixed-resolution input, and performs inference using the restoration point β^* . The inference results are then returned to the mobile device for local state updates. In the remainder of this paper, we use *object detection* as a case study to detail the key system designs of ViTMALis, as it is the most widely studied task in existing MVA research.

C. Accuracy-Oriented Region Selection

Let \mathcal{R} denote the set of all decision regions. For each frame scheduled for offloading, we need to determine the binary downsampling mask $\mathbf{B} \in \{0, 1\}^{|\mathcal{R}|}$, where the j -th entry equals 1 if decision region j is downsampled, with the objective of reducing E2E offloading latency while minimizing inference accuracy degradation. Since the optimal choice of \mathbf{B} varies with video content, dynamically adapting the mask for each frame is essential. Theoretically, we can make a downsampling decision for each region independently, yielding $2^{|\mathcal{R}|}$ possible combinations. As navigating this exponentially large decision space is computationally prohibitive for real-time applications, we propose a heuristic approach to streamline the selection process.

To this end, we analyze the content characteristics of MVA frames. Due to camera mobility, video content in MVA often exhibits substantial dynamics and structural complexity. To quantify the characteristics of each decision region j , we define two metrics: *motion* (m_j) and *task relevance* (ρ_j). The motion m_j is estimated by the *Region Motion Analyzer* using a lightweight background subtraction model [33] and is calculated as the ratio of foreground pixels (i.e., pixels exhibiting significant motion) in region j to the total number of foreground pixels in the frame. The task relevance ρ_j reflects the importance of the region to the downstream prediction task



Fig. 7. An example of identifying region types based on background subtraction and local tracking.

and is computed based on task-specific outputs. For object detection, ρ_j corresponds to *regional object density*, defined as the fraction of objects whose bounding boxes partially or fully overlap region j .

Based on these metrics, we observe that regions within a frame can be systematically classified into three categories: (1) *static background regions (SBRs)*, characterized by low motion and low task relevance, which remain nearly unchanged and are minimally affected by camera motion over extended durations (e.g., sky or sea); (2) *camera-induced motion regions (CMRs)*, characterized by high motion but low task relevance, containing objects that are stationary in the real world (e.g., trees or buildings) but appear to move due to camera mobility; and (3) *dynamic object regions (DORs)*, characterized by high motion and high task relevance, containing objects capable of independent movement (e.g., pedestrians or vehicles). We leverage a motion threshold δ^m and a task relevance threshold δ^ρ to identify the category of a given region j . If $m_j < \delta^m$, the region is classified as an SBR. Otherwise, if $\rho_j > \delta^\rho$, it is classified as a DOR. Regions meeting neither condition are classified as CMRs. Fig. 7 illustrates an example of this region type assignment.

Given that downsampling DORs risks severe accuracy degradation, we strictly preserve these regions at full resolution. To guide the downsampling strategy, we define a downsampling type variable $\tau_d \in \{0, 1, 2\}$, where each value specifies a target set of regions for downsampling: no downsampling (0), CMRs only (1), or both CMRs and SBRs (2). Type 0 corresponds to high-quality frame offloading, typically reserved for scenarios with abundant network and computational resources. We exclude the option of downsampling only SBRs, as our empirical observations consistently show that it yields suboptimal results compared to the option of downsampling only CMRs. This is because SBRs generally consist of low-frequency content that can be efficiently compressed even at full resolution, whereas downsampling often high-frequency CMRs provides significantly larger bandwidth savings for a similar impact on accuracy.

Let ϕ denote the region-type map of the current frame, where each element $\phi_j \in \{\text{SBR}, \text{CMR}, \text{DOR}\}$ specifies the type of decision region j . Once τ_d is determined, the binary downsampling mask \mathbf{B} is generated as $\mathbf{B} = f_{\tau_d}(\phi)$, where f_{τ_d} assigns a value of 1 to all regions belonging to the categories targeted for downsampling by τ_d . Crucially, even for a fixed τ_d , \mathbf{B} varies across frames, as ϕ evolves dynamically with

camera motion.

D. Content-Aware Performance Estimation

Let $N_d = \sum_{j \in \mathcal{R}} B_j$ denote the number of downsampled decision regions specified by \mathbf{B} . Our large-scale offline profiling on the target mobile device shows that the frame encoding delay T^{enc} depends on both the number of downsampled regions N_d and the compression quality parameter λ . We therefore use the profiled results $T^{\text{enc}}(N_d, \lambda)$ to directly estimate the encoding delay on the target device. Although the decoding delay T^{dec} varies slightly across configurations, it remains relatively small compared with other delay components. We thus approximate T^{dec} using the mean value measured from offline profiling on the server.

The server-side model inference delay T^{inf} depends on the restoration point β and the input token sequence length, which is determined by N_d . For a fixed β , our profiling results reveal an approximately linear relationship between N_d and inference delay. Therefore, we estimate T^{inf} using a set of linear models $\text{LM}_\beta^{\text{inf}}(N_d)$, where each model corresponds to a specific restoration point and is parameterized based on offline profiling on the target server. Regarding network latency, since vision model inference results are typically small (only a few hundred bytes), the result download delay is dominated by propagation rather than transmission. We thus approximate the total propagation delay (for both frame upload and result download) as the round-trip time (RTT), denoted as L^{net} .

The frame upload delay is primarily determined by the compressed frame size and the current network throughput. While the mean upload throughput U can be estimated using existing methods [34]–[36], estimating the compressed data size $S(\mathbf{c})$ is more challenging, as it depends on N_d , λ , and specific frame content. To address this, we use the sum of motion values in all downsampled regions, denoted as $m^d = \sum_{j \in \mathcal{R}} B_j m_j$, as a proxy for the content characteristics of the downsampled regions. To capture global content dynamics, we define the normalized frame motion m^f as the ratio of the foreground pixels to the total number of pixels in the image. We then train a lightweight multilayer perceptron (MLP) to estimate $S(\mathbf{c})$:

$$\hat{S}(\mathbf{c}) = \text{MLP}^{\text{size}}(\tau_d, N_d, m^d, m^f, \lambda) \quad (1)$$

With all latency components estimated, the Performance Estimator predicts the E2E offloading latency $T(\mathbf{c})$ as:

$$\hat{T}(\mathbf{c}) = \hat{T}^{\text{enc}}(N_d, \lambda) + \frac{\hat{S}(\mathbf{c})}{\hat{U}} + \hat{T}^{\text{dec}} + \text{LM}_\beta^{\text{inf}}(N_d) + \hat{L}^{\text{net}} \quad (2)$$

The inference accuracy of the server-side model $A(\mathbf{c})$ is affected by all configuration knobs in \mathbf{c} as well as by frame content relevant to the dense prediction task. To capture this content dependency, we derive two statistics from the regional task relevance ρ_j : the mean $\mu(\rho_j)$ and the standard deviation $\sigma(\rho_j)$ computed over all decision regions $j \in \mathcal{R}$. Specifically, $\mu(\rho_j)$ reflects how widely task-relevant content is distributed across the image, whereas $\sigma(\rho_j)$ measures the degree of spatial concentration, indicating whether the task-relevant content is evenly dispersed or clustered within specific regions. These statistics, together with motion features and configuration parameters, are input to a lightweight MLP model that estimates the inference accuracy for each \mathbf{c} :

$$\hat{A}(\mathbf{c}) = \text{MLP}^{\text{acc}}(\mathbf{c}, N_d, m^d, m^f, \mu(\rho_j), \sigma(\rho_j)) \quad (3)$$

E. Offload Configuration Selection

Algorithm 1 details how the Offload Optimizer selects the configuration \mathbf{c}^* for each frame scheduled for offloading. The algorithm begins by classifying each decision region j into SBR, CMR, or DOR based on m_j and ρ_j (line 1). It then evaluates the estimated E2E offloading latency $\hat{T}(\mathbf{c})$ and inference accuracy $\hat{A}(\mathbf{c})$ for each candidate configuration \mathbf{c} (lines 2-11). In our implementation, the Offload Optimizer estimates the average upload throughput and network latency by averaging observations from the two most recent offloading operations. This short-window averaging provides a low overhead baseline suitable for our target scenarios, and our framework supports the direct integration of more advanced prediction methods (e.g., Transformer-based models) if desired.

With the estimated E2E offloading latency and inference accuracy, the Offload Optimizer identifies the subset of configurations on the *Pareto frontier* (line 12), where each configuration is Pareto optimal in the sense that improving one performance objective (e.g., reducing latency) necessarily degrades the other (e.g., reducing accuracy). If only a single configuration lies on the frontier, it simultaneously achieves the minimum E2E offloading latency and the maximum inference accuracy, and is therefore selected (lines 13-14). Otherwise, selection is guided by the system's current status.

Specifically, the Offload Optimizer evaluates two runtime metrics: η , the *frame interval* since the last offloaded frame, and κ , the *tracking retention ratio*, defined as the proportion of objects that have been continuously tracked since the most recent reinitialization of the Local Tracker. A high η or a low κ indicates increased urgency for low-latency offloading to ensure the freshness of rendering results. Accordingly, if η exceeds a staleness threshold δ^η (i.e., a long interval since the last offload), or if κ falls below a retention threshold δ^κ (i.e., poor tracking retention), the Offload Optimizer selects the configuration with the lowest estimated E2E offloading latency to enable rapid local state updates (lines 16-17). In all other cases, it selects the configuration at the *knee point* [37] of the Pareto frontier (lines 18-19). This point reflects the most favorable balance between the E2E offloading latency and inference accuracy, beyond which further improvement in one objective would incur significant degradation in the other.

Algorithm 1: Offload Configuration Selection

Data: $m^f, m_j, \rho_j, \mathcal{C}, \hat{U}, \hat{L}^{\text{net}}, \kappa, \eta$
Result: Selected configuration \mathbf{c}^*

```

1  $\phi \leftarrow$  Classify  $j \in \mathcal{R}$  into SBR/CMR/DOR based on  $m_j$  and
    $\rho_j$ ;
2  $\mathcal{Z} \leftarrow \emptyset$ ;
3 foreach  $\mathbf{c} \in \mathcal{C}$  do
4   Extract parameters  $\tau_d, \lambda, \beta$  from  $\mathbf{c}$ ;
5    $\mathbf{B} \leftarrow f_\tau(\tau_d, \phi)$ ;
6    $N_d \leftarrow \sum_{j \in \mathcal{R}} B_j$  ;
7    $m^d \leftarrow \sum_{j \in \mathcal{R}} B_j m_j$  ;
8    $\hat{S}(\mathbf{c}) \leftarrow \text{MLP}^{\text{size}}(\tau_d, N_d, m^d, m^f, \lambda)$  ;
9    $\hat{T}(\mathbf{c}) \leftarrow \text{ComputeLatency}(\mathbf{c}, \hat{S}, \hat{U}, \hat{L}^{\text{net}})$  ; // Eq. (2)
10   $\hat{A}(\mathbf{c}) \leftarrow \text{MLP}^{\text{acc}}(\mathbf{c}, N_d, m^d, m^f, \mu(\rho_j), \sigma(\rho_j))$  ;
11   $\mathcal{Z} \leftarrow \mathcal{Z} \cup \{(\mathbf{c}, \hat{T}(\mathbf{c}), \hat{A}(\mathbf{c}))\}$ ;
12  $\mathcal{C}^{\text{opt}} \leftarrow \text{ParetoFrontier}(\mathcal{Z})$ ;
13 if  $|\mathcal{C}^{\text{opt}}| = 1$  then
14    $\mathbf{c}^* \leftarrow$  the unique element of  $\mathcal{C}^{\text{opt}}$ ;
15 else
16   if  $\kappa < \delta^\kappa$  or  $\eta > \delta^\eta$  then
17      $\mathbf{c}^* \leftarrow \arg \min_{(\mathbf{c}, \hat{T}, \hat{A}) \in \mathcal{C}^{\text{opt}}} \hat{T}$ ;
18   else
19      $\mathbf{c}^* \leftarrow \text{KneePoint}(\mathcal{C}^{\text{opt}})$ ;
20 return  $\mathbf{c}^*$ ;

```

V. SYSTEM IMPLEMENTATION

We implemented a prototype of ViTMAlis using commodity hardware. The mobile client is an NVIDIA Jetson Orin Nano [38], a representative embedded AI computing platform, while the edge server is a desktop workstation equipped with an Intel i9-13900K CPU and an NVIDIA GeForce RTX 5090 GPU. Both the mobile device and server run Ubuntu 22.04 and connect via a TP-Link AX3000 router. Without network shaping, this setup achieves close to 1 Gbps throughput. To evaluate performance under realistic network conditions, we utilize the network emulation tool Mahimahi [39]. Specifically, Mahimahi replays real-world 4G and 5G traces to emulate time-varying uplink throughput and network latency between the mobile device and the server. For data transport, we employ ZeroMQ [40] due to its lightweight message-passing capabilities and low overhead. Despite this, the communication layer of ViTMAlis is protocol-agnostic and supports seamless integration with other transport methods.

The prototype is implemented in Python, and the MLP models are trained and deployed with PyTorch. We use OpenCV [41] to encode offloaded frames as JPEG and decode them on receipt. For the Local Tracker, a lightweight implementation is critical, as it must simultaneously track multiple objects and perform additional catch-up tracking [25] (i.e., aligning delayed remote results with the current live video) for intermediate frames generated during offloading. After evaluating various approaches [1], [25], [42], we selected an optical flow-based tracking method [25], as it provides the most effective balance between tracking accuracy and speed.

TABLE I
VIDEO SOURCES USED IN THIS PAPER

Name	Source	Illumination	Motion	Recording Scenario
walkS	YouTube [43]	Sunny	Low	A sunny countryside walk
walkR	YouTube [44]	Rainy	Low	A city walk in gentle rain
walkB	Self-shot	Artificial lighting	Low	A walk inside a bustling commercial building
cycleS	YouTube [45]	Sunny	High	A sunny cycling from Brentwood to Hollywood
driveN	YouTube [46]	Night	High	A night drive around Mexico City

VI. EVALUATION

A. Evaluation Setup

Video dataset. Table I summarizes the videos used for evaluation. To ensure comprehensive evaluation, the dataset encompasses diverse motion patterns, lighting conditions (day/night, indoor/outdoor), and weather scenarios. The videos were either sourced from YouTube [43]–[46] or recorded by us using a body-worn Insta360 GO 3S camera [47]. Importantly, all videos were captured with moving cameras to closely reflect the content characteristics of MVA. From each video source, we extracted a 60-second video clip for model training and profiling, and another 300-second video clip for system evaluation. In total, our evaluation dataset comprises 45,000 frames.

Experimental testbed. To ensure experimental reproducibility and fair comparisons under identical video content during evaluation, we replay the pre-recorded video clips on the mobile device to emulate live camera input. In particular, to simulate a real-world camera operating at 1080p and 30 FPS, we leverage the *hardware decoding accelerator* on the NVIDIA Jetson Orin Nano and construct a GStreamer [48] pipeline for efficient video decoding. Since the hardware decoding speed exceeds 30 FPS, we employ a pacing queue to regulate frame delivery to the Camera Buffer, ensuring a strict real-time input rate of 30 FPS.

Server-side inference models. We use ViTDet-L for evaluation, which is pre-trained with an image patch size of 16×16 pixels. To facilitate frame region partitioning, we fine-tune the pre-trained model using a reduced window size of 9×9 . The default downsampling ratio d is set to 2, meaning that each decision region consists of 18×18 image patches (recall §III-A).

Network traces. The trace dataset is constructed from multiple public sources [49]–[51] to capture diverse mobility patterns. It comprises 60 traces in total, evenly divided between 4G and 5G networks. Each trace spans 300 seconds to align with the test video duration and varies at a fine-grained temporal resolution of 1 second. The average upload throughput across traces ranges from 10.4 to 36.4 Mbps for 4G and from 12.2

to 135.5 Mbps for 5G. The average network latency is 39 ms for 4G and 34 ms for 5G.

Configuration and hyperparameter settings. For the compression quality parameter λ , we consider 7 options ranging from 70 to 100 (the highest quality), with an increment of 5. β has 5 candidate options, as introduced in §III-B. Note that when $\tau_d = 0$, β is fixed to 0, as the absence of downsampled regions implies that no resolution restoration is required. Based on profiling statistics, the motion threshold δ^m is set to 0.001 to effectively distinguish SBRs from other region types. The relevance threshold δ^p is set to 0 to prioritize accuracy by treating all object-relevant regions as critical. The thresholds δ^η and δ^κ are empirically set to 30 and 0.7, respectively. Finally, we utilize the Optuna hyperparameter optimization framework [52] to optimize the MLP architectures. Consequently, both MLP^{size} and MLP^{acc} are configured with three layers consisting of 128, 64, and 1 neurons, respectively.

Performance metrics. To evaluate the overall system performance, we focus on the following key metrics:

- *Rendering accuracy.* It reflects the user-perceived quality of experience (QoE). It is defined as the F1 score between the final rendered results (displayed to the user) and the corresponding ground-truth detections, aggregated across all frames in a video. Ground-truth detections are obtained by running the original ViTDet-L model on raw full-resolution video frames.
- *E2E offloading latency.* This is the total duration from the start of frame encoding to the reception of the inference result. This metric measures the freshness of the returned inference results, which directly determines the timeliness of local state updates.
- *Inference accuracy.* This metric is defined as the F1 score between the server-side model’s inference results and the corresponding ground-truth results, aggregated over all offloaded frames in a video.
- *Offloading interval.* This measures the frame stride between two consecutively offloaded frames.

Baselines. We consider the following baselines:

- *Back2Back:* A standard baseline from prior work [1], [53] that offloads the most recently captured frame immediately upon receiving the inference result for the previous offload. If a frame’s remote inference result is unavailable by its rendering deadline, the most recent remote result is reused.
- *TrackB2B:* An accuracy-centric baseline. It represents the canonical edge-assisted MVA paradigm [3], [25] by augmenting Back2Back with a local tracker. The tracker maintains rendering accuracy by generating predictions when remote inference results are unavailable due to prolonged offloading latency. Furthermore, it offloads and performs inference on full-resolution frames to preserve inference accuracy.
- *TrackRoI:* A content-aware baseline. It represents standard RoI-based compression strategies [16], [54] that adapt to video content. Built upon TrackB2B, it reduces data transmission by masking out non-RoI regions, which correspond to decision regions not classified as DORs in

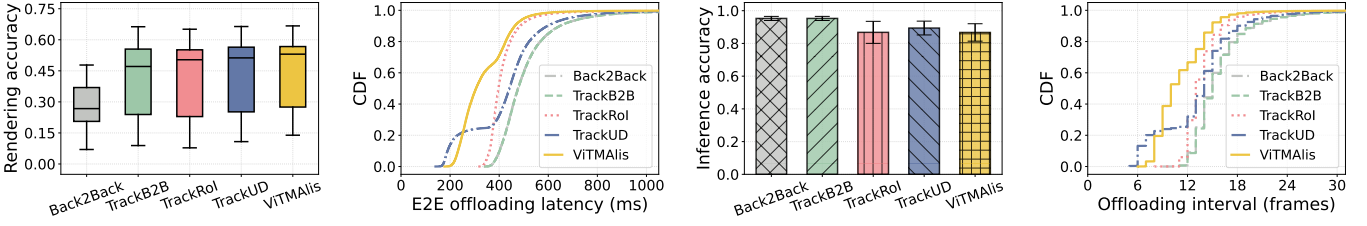


Fig. 8. Overall performance of the different solutions. The figures show statistics for all 300 video-trace pairs. For the inference accuracy, bar heights represent the mean values averaged across all pairs, while error bars denote the standard deviation.

our setting.

- **TrackUD:** A latency-adaptive baseline. Inspired by adaptive video streaming [55], [56], it builds upon TrackB2B and dynamically adjusts frame resolution to mitigate high system delays. Specifically, it monitors the most recent E2E offloading latency. If the latency exceeds an empirically determined threshold of 15 frame intervals, the frame is uniformly downsampled by a factor of 2 to regain synchronization with the live input. Otherwise, the full resolution is used to prioritize inference accuracy.

All baselines utilize a default JPEG compression quality of 95. This setting aligns with standard practice (e.g., the default value in OpenCV) and was empirically found to yield the best performance for strong baselines.

B. Overall System Performance

Fig. 8 compares the overall performance of all evaluated solutions. As shown, Back2Back yields the lowest rendering accuracy, with a median value of 0.268. Although it maintains a high mean inference accuracy of about 0.953, its long E2E offloading latency causes the returned inference results to become outdated, ultimately degrading the rendering accuracy. Specifically, approximately 40% of the offloading intervals exceed 15 frames, indicating that the rendered view lags behind the ground truth by at least 15 frames. The accuracy-centric baseline TrackB2B shares the same offloading behavior as Back2Back, yet its median rendering accuracy increases substantially to 0.471 due to the use of the local tracker.

Compared with TrackB2B, TrackRoI further increases the median rendering accuracy to 0.504 through its content-aware masking mechanism. Masking out partial frame regions inevitably causes a drop in the inference accuracy of offloaded frames, decreasing the mean inference accuracy from 0.953 to 0.868. However, this also reduces the E2E offloading latency, enhancing the freshness of the returned remote inference results and ultimately contributing to the improved rendering accuracy. As shown in Fig. 9, the reduction in E2E offloading latency for TrackRoI primarily stems from lower network communication delay, since masking out partial frame regions reduces the amount of data transmitted over the network. In contrast, the latency-adaptive baseline TrackUD reduces both network delay and inference delay compared with TrackB2B. The joint reduction in network and inference delay effectively decreases the E2E offloading latency under poor network conditions, thereby ensuring the freshness of the remote inference results. Despite the drop in mean inference accuracy caused

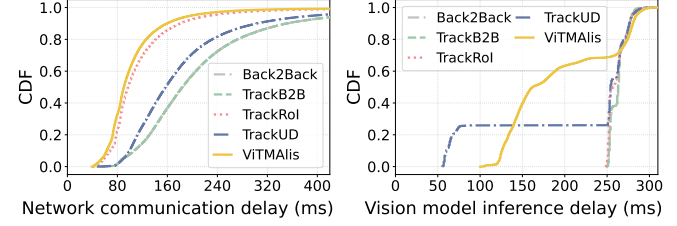


Fig. 9. In-depth delay examination.

by inference on uniformly downsampled frames, the final rendering accuracy (0.512) is higher than that of TrackRoI.

Fig. 9 reveals that our dynamic mixed-resolution inference strategy reduces the median vision model inference delay from over 263 ms to 162 ms. Simultaneously, by strategically optimizing mixed-resolution decisions on the mobile device, ViTMAlis reduces the median network communication delay to 90 ms, representing nearly a 51% reduction compared to Back2Back and TrackB2B. Together, these improvements substantially reduce the E2E offloading latency and offloading interval, enabling faster feedback and more frequent local state updates to ensure freshness. Thanks to our accuracy-oriented region selection strategy, the drop in mean inference accuracy remains moderate (0.867) and comparable to that of TrackRoI and TrackUD. Overall, ViTMAlis achieves the highest median rendering accuracy of 0.530, validating that our content- and network-aware framework effectively balances offloading quality and timeliness.

C. Codec Delays and Overhead Analysis

Fig. 10 compares the encoding and decoding delays across different solutions. Among the baselines, TrackUD achieves a notably lower first quartile in codec delays compared to Back2Back and TrackB2B. This is because a portion of the frames are processed at a downsampled resolution. In contrast, TrackRoI and ViTMAlis exhibit slightly higher median encoding delays due to the preprocessing overhead required to generate masked or mixed-resolution frames. However, the reduced pixel count in these frames leads to lower median decoding delays compared to other baselines, albeit with higher variance due to the content-dependent nature of the masks. Quantitatively, the median total codec delays for Back2Back, TrackB2B, TrackRoI, TrackUD, and ViTMAlis are 30, 30, 38, 30, and 39 ms, respectively. As shown, ViTMAlis's codec overhead is comparable to that of the content-aware baseline TrackRoI and introduces only a marginal increase over the

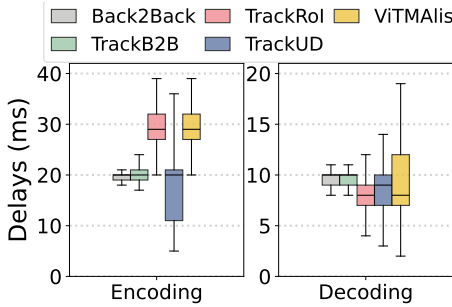


Fig. 10. Codec delays

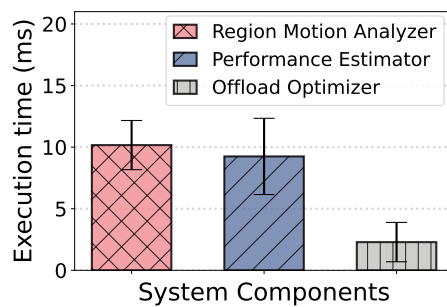


Fig. 11. System Overhead

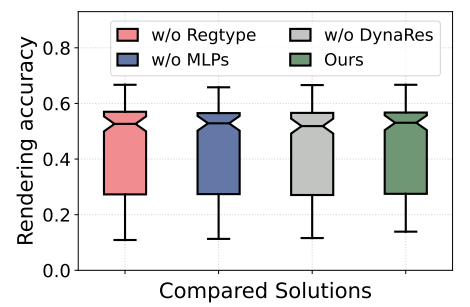


Fig. 12. Ablation Study

TABLE II
PERFORMANCE COMPARISON OF DIFFERENT ESTIMATION METHODS.

Methods	Prediction type	MAE ↓	RMSE ↓	MAPE ↓	R ² ↑
Linear Regression	Size (KiB)	98.0	131.6	51.6	0.612
	Accuracy	0.164	0.206	48.6	0.549
Offline Mean	Size (KiB)	53.3	83.1	26.8	0.846
	Accuracy	0.082	0.122	22.3	0.841
MLP (ours)	Size (KiB)	38.6	67.4	17.3	0.898
	Accuracy	0.078	0.114	17.7	0.860

other baselines, a negligible cost given the significant gains in rendering accuracy.

ViTMAlis’s system overhead primarily stems from three key components: the Region Motion Analyzer, the Performance Estimator, and the Offload Optimizer. As illustrated in Fig. 11, the Region Motion Analyzer incurs an average processing time of 10 ms per frame on the Jetson Orin Nano GPU. Note that this component is implemented as a separate thread that executes in parallel with the Local Tracker, thereby introducing negligible additional delay compared to the tracking-enabled baselines. The Performance Estimator employs two lightweight MLP models to predict compressed data size and inference accuracy, requiring only 9 ms on average to evaluate all candidate configurations. Finally, the Offload Optimizer executes Algorithm 1 to determine the optimal configuration, a process that is highly efficient and takes approximately 2 ms on average.

D. Ablation Study

To validate the effectiveness of our design choices, we conduct a two-stage ablation study. First, we evaluate the prediction accuracy of the Performance Estimator to justify the use of MLP-based modeling. Second, we assess the impact of removing key system components on the rendering accuracy.

Accuracy of Performance Estimation. We compare our MLP-based estimator against two alternative approaches: (1) *Linear Regression*, which employs the identical set of input features as our MLP models but attempts to predict performance targets using linear functions; and (2) *Offline Mean*, a static baseline that estimates the compressed data size and inference accuracy using the average values observed during offline profiling. To ensure generalization, all estimators were

trained or calibrated on a composite dataset that aggregates the profiling clips from all evaluated domains, thereby mitigating scenario-specific bias.

Table II summarizes the results across four metrics: Mean Absolute Error (MAE), Root Mean Square Error (RMSE), Mean Absolute Percentage Error (MAPE), and the Coefficient of Determination (R²). As shown, Linear Regression exhibits a poor fit, with R² values of only 0.612 for data size and 0.549 for accuracy. This confirms that the relationship between the input features and performance targets is highly non-linear and cannot be captured by simple linear functions. While the Offline Mean baseline improves the R² to approximately 0.84, it still suffers from high error rates (MAPE > 22%) because it ignores the dynamic variations in video content.

In contrast, our MLP-based estimator achieves the best performance across all metrics. It improves the R² for data size prediction to 0.898 and reduces the MAPE to 17.3%. Similarly, for accuracy prediction, it achieves the lowest MAE (0.078) and RMSE (0.114). These results demonstrate that our lightweight MLPs effectively capture the complex, non-linear dependencies between input features and performance targets. Furthermore, we conducted cross-domain validation (training on walking scenarios while testing on driving/cycling) to assess robustness. The results indicate performance drops of less than 5%. We attribute this robustness to the fact that our estimator relies on abstract statistical features rather than domain-specific visual patterns, thereby generalizing effectively across diverse mobility scenarios.

Impact on System Performance. We next evaluate how key system components contribute to the overall performance. Specifically, we compare our full system against three ablated variants: (1) w/o RegType, which removes fine-grained region classification and instead downsamples all non-DORs; (2) w/o MLPs, which substitutes the content-aware Performance Estimator with the static Offline Mean estimator described above; and (3) w/o DynaRes, which disables the dynamic resolution restoration mechanism, deferring feature map upsampling until the final layer of the ViT backbone.

Fig. 12 presents the rendering accuracy distribution for our proposed solution and its ablated variants. As shown, the ablations reduce the median rendering accuracy from 0.530 (Full System) to 0.526 (w/o RegType), 0.528 (w/o MLPs), and 0.518 (w/o DynaRes). We observe that while all variants achieve lower mean E2E offloading latency, these gains are achieved at the expense of drops in mean inference accuracy,

which ultimately degrades the final rendering quality.

For w/o RegType and w/o DynaRes, this degradation stems from an inherently constrained decision space. Lacking the fine-grained control provided by the corresponding components, the optimizer is precluded from exploiting resource-efficient configurations that are sufficiently accurate. In contrast, w/o MLPs retains access to the full configuration space but is limited by its reliance on static, non-adaptive profiling. Because the fixed performance estimates fail to capture real-time variations in video content complexity, the optimizer becomes rigid, often biasing the selection toward a limited set of suboptimal configurations rather than adapting to the specific frame. Despite these drops, it should be noted that all ablated variants still outperform the baselines. This confirms that even without these specific optimizations, our core mixed-resolution compression and inference strategy remains robust, effectively optimizing the accuracy-latency trade-off for ViT-backboned MVA systems.

VII. RELATED WORK

A. Edge-Assisted Mobile Video Analytics

Recent research in MVA progressively addresses the latency and scalability limits of edge offloading through pipeline optimization, distributed computing infrastructure, and multi-objective scheduling. Foundational work by Liu et al. [17] minimizes single-task (i.e., object detection) offloading latency by decoupling the rendering and offloading pipelines. They introduce *dynamic RoI encoding* and *parallel streaming and inference* to accelerate offloading, while employing motion vector-based local tracking to maintain detection accuracy. To accommodate the increased computational demands of high-resolution videos, Elf [18] enhances scalability by partitioning frames based on region proposals and offloading partial inference tasks in parallel across multiple servers. To address the offloading path selection complexity in such distributed environments, FPSelector [57] optimizes multipath transmission using reinforcement learning, specifically managing the data dependencies between sequential sub-tasks to prevent invalid offloading decisions.

Moving beyond single-task optimization, AccuMO [2] orchestrates resource allocation in multitask AR scenarios, such as simultaneous depth estimation and odometry. It maximizes overall application accuracy by dynamically balancing offloading frequencies and local execution based on the sensitivity of task accuracy to offloading frequency and frame content. Finally, to address server-side scalability, ARISE [3] coordinates the offloading schedules of multiple concurrent clients to maximize server batching efficiency while strictly satisfying individual service level agreements. Despite these advancements, existing works predominantly rely on CNN-backboned vision models or traditional computer vision algorithms. They therefore lack specialized optimizations for ViTs, failing to address the unique computational challenges or leverage the opportunities arising from their specific architecture.

B. Vision Transformer Inference Acceleration

To mitigate the quadratic computational cost of ViTs, extensive research has been dedicated to model-centric acceler-

ation techniques, such as token pruning, token merging, and mixed-resolution inference. For instance, DynamicViT [28] introduces a learnable prediction module to selectively drop less informative tokens hierarchically at intermediate layers, thereby reducing redundancy. ToMe [29] progressively merges similar tokens using a bipartite matching algorithm to decrease token count without requiring retraining. Quadformer [23] leverages a Quadtree algorithm to construct mixed-resolution token sequences, recursively splitting the image into varying patch sizes based on importance estimated by a saliency scorer. While these techniques successfully reduce inference complexity, they typically assume that data is locally available and computational resources are abundant, focusing solely on reducing theoretical FLOPs. As such, they often overlook the resource limitations of mobile devices and the network transmission costs inherent to offloading scenarios.

Complementing the algorithmic optimizations, system-level research has focused on collaborative inference and adaptive offloading to accelerate ViTs in practical deployments. In the device-to-cloud domain, Janus [58] introduces a framework that dynamically combines token pruning with adaptive model splitting to maintain performance under fluctuating network conditions. Also targeting cloud offloading, LVMScissor [59] addresses the intermediate data expansion of large vision models by employing horizontal model parallelism and heuristic scheduling to minimize E2E latency. Shifting focus to device-to-device collaboration, SPViT [60] proposes an adaptive splitting framework that partitions ViT heads and neurons across multiple local mobile devices to parallelize inference. While effective, these approaches typically rely on complex partitioning or structural pruning, which introduce significant synchronization overheads or require invasive architectural changes. Distinct from these directions, our work introduces a non-intrusive mixed-resolution strategy that optimizes token representation at the input level, reducing both transmission and computation costs without splitting the model.

VIII. CONCLUSION

In this paper, we presented ViTMAlis, a ViT-native offloading framework designed to tackle the substantial resource and latency challenges of edge-assisted MVA with ViT-backboned models. Leveraging the input-agnostic nature of ViTs, ViTMAlis introduces a mixed-resolution inference strategy that dynamically balances E2E offloading latency and inference accuracy based on real-time video content and network conditions. The framework incorporates lightweight on-device motion analysis and local tracking to enable accuracy-oriented region downsampling and configuration optimization. Extensive experiments on real-world mobile videos and network traces demonstrate that ViTMAlis significantly reduces E2E offloading latency while delivering superior rendering accuracy compared to strong baselines.

REFERENCES

- [1] J. Meng, Z. J. Kong, Y. C. Hu, M. G. Choi, and D. Lal, “Do we need sophisticated system design for edge-assisted augmented reality?” in *Proceedings of the 5th International Workshop on Edge Systems, Analytics and Networking (EdgeSys)*, 2022, pp. 7–12.

[2] Z. J. Kong, Q. Xu, J. Meng, and Y. C. Hu, “Accumo: Accuracy-centric multitask offloading in edge-assisted mobile augmented reality,” in *Proceedings of the 29th Annual International Conference on Mobile Computing and Networking (MobiCom)*, 2023, pp. 1–16.

[3] Z. J. Kong, Q. Xu, and Y. . Hu, “Arise: High-capacity ar offloading inference serving via proactive scheduling,” in *Proceedings of the 22nd Annual International Conference on Mobile Systems, Applications and Services (MobiSys)*, 2024, pp. 451–464.

[4] A. Dosovitskiy, L. Beyer, A. Kolesnikov, D. Weissenborn, X. Zhai, T. Unterthiner, M. Dehghani, M. Minderer, G. Heigold, S. Gelly *et al.*, “An image is worth 16x16 words: Transformers for image recognition at scale,” *arXiv preprint arXiv:2010.11929*, 2020.

[5] A. Vaswani, N. Shazeer, N. Parmar, J. Uszkoreit, L. Jones, A. N. Gomez, Ł. Kaiser, and I. Polosukhin, “Attention is all you need,” *Proceedings of the 31st Conference on Neural Information Processing System (NeurIPS)*, vol. 30, 2017.

[6] R. Strudel, R. Garcia, I. Laptev, and C. Schmid, “Segmenter: Transformer for semantic segmentation,” in *Proceedings of the IEEE/CVF international conference on computer vision (ICCV)*, 2021, pp. 7262–7272.

[7] Y. Li, H. Mao, R. Girshick, and K. He, “Exploring plain vision transformer backbones for object detection,” in *European Conference on Computer Vision (ECCV)*, 2022, pp. 280–296.

[8] Y. Xu, J. Zhang, Q. Zhang, and D. Tao, “Vitpose: Simple vision transformer baselines for human pose estimation,” *Advances in Neural Information Processing Systems (NeurIPS)*, vol. 35, pp. 38571–38584, 2022.

[9] A. Kirillov, E. Mintun, N. Ravi, H. Mao, C. Rolland, L. Gustafson, T. Xiao, S. Whitehead, A. C. Berg, W.-Y. Lo *et al.*, “Segment anything,” in *Proceedings of the IEEE/CVF International Conference on Computer Vision (ICCV)*, 2023, pp. 4015–4026.

[10] N. Ravi, V. Gabeur, Y.-T. Hu, R. Hu, C. Ryali, T. Ma, H. Khedr, R. Rádile, C. Rolland, L. Gustafson *et al.*, “Sam 2: Segment anything in images and videos,” *arXiv preprint arXiv:2408.00714*, 2024.

[11] Y. Zhang, X. Huang, J. Ma, Z. Li, Z. Luo, Y. Xie, Y. Qin, T. Luo, Y. Li, S. Liu *et al.*, “Recognize anything: A strong image tagging model,” in *Proceedings of the IEEE/CVF Conference on Computer Vision and Pattern Recognition (CVPR)*, 2024, pp. 1724–1732.

[12] A. Radford, J. W. Kim, C. Hallacy, A. Ramesh, G. Goh, S. Agarwal, G. Sastry, A. Askell, P. Mishkin, J. Clark *et al.*, “Learning transferable visual models from natural language supervision,” in *Proceedings of the 38th International Conference on Machine Learning (ICML)*. PMLR, 2021, pp. 8748–8763.

[13] M. Maaz, H. Rasheed, S. Khan, and F. S. Khan, “Video-chatgpt: Towards detailed video understanding via large vision and language models,” in *Proceedings of the 62nd Annual Meeting of the Association for Computational Linguistics (ACL)*, 2024.

[14] H. Zhang, G. Ananthanarayanan, P. Bodik, M. Philipose, P. Bahl, and M. J. Freedman, “Live video analytics at scale with approximation and delay-tolerance,” in *Proceedings of the 14th USENIX Symposium on Networked Systems Design and Implementation (NSDI)*, 2017, pp. 377–392.

[15] Y. Li, A. Padmanabhan, P. Zhao, Y. Wang, G. H. Xu, and R. Neotravali, “Reducto: On-camera filtering for resource-efficient real-time video analytics,” in *Proceedings of the Annual conference of the ACM Special Interest Group on Data Communication on the applications, technologies, architectures, and protocols for computer communication (SIGCOMM)*, 2020, pp. 359–376.

[16] S. Liu, T. Wang, J. Li, D. Sun, M. Srivastava, and T. Abdelzaher, “Adamask: Enabling machine-centric video streaming with adaptive frame masking for dnn inference offloading,” in *Proceedings of the 30th ACM International Conference on Multimedia (MM)*, 2022, pp. 3035–3044.

[17] L. Liu, H. Li, and M. Gruteser, “Edge assisted real-time object detection for mobile augmented reality,” in *The 25th annual international conference on mobile computing and networking (MobiCom)*, 2019, pp. 1–16.

[18] W. Zhang, Z. He, L. Liu, Z. Jia, Y. Liu, M. Gruteser, D. Raychaudhuri, and Y. Zhang, “Elf: Accelerate high-resolution mobile deep vision with content-aware parallel offloading,” in *Proceedings of the 27th Annual International Conference on Mobile Computing and Networking (MobiCom)*, 2021, pp. 201–214.

[19] K. Teja C.-V., S. Mittal, M. Emani, V. Vishwanath, and A. K. Somani, “A survey of techniques for optimizing transformer inference,” *Journal of Systems Architecture*, vol. 144, p. 102990, 2023.

[20] Z. Kong, P. Dong, X. Ma, X. Meng, W. Niu, M. Sun, X. Shen, G. Yuan, B. Ren, H. Tang *et al.*, “Svit: Enabling faster vision transformers via latency-aware soft token pruning,” in *European Conference on Computer Vision (ECCV)*. Springer, 2022, pp. 620–640.

[21] M. Fayyaz, S. A. Koohpayegani, F. R. Jafari, S. Sengupta, H. R. V. Jozé, E. Sommerlade, H. Pirsavash, and J. Gall, “Adaptive token sampling for efficient vision transformers,” in *European Conference on Computer Vision (ECCV)*. Springer, 2022, pp. 396–414.

[22] J. B. Haurum, S. Escalera, G. W. Taylor, and T. B. Moeslund, “Which tokens to use? investigating token reduction in vision transformers,” in *Proceedings of the IEEE/CVF International Conference on Computer Vision (ICCV)*, 2023, pp. 773–783.

[23] T. Ronen, O. Levy, and A. Golbert, “Vision transformers with mixed-resolution tokenization,” in *Proceedings of the IEEE/CVF Conference on Computer Vision and Pattern Recognition (CVPR)*, 2023, pp. 4612–4621.

[24] J. D. Havtorn, A. Royer, T. Blankevoort, and B. E. Bejnordi, “Msvit: Dynamic mixed-scale tokenization for vision transformers,” in *Proceedings of the IEEE/CVF International Conference on Computer Vision (ICCV)*, 2023, pp. 838–848.

[25] T. Y.-H. Chen, L. Ravindranath, S. Deng, P. Bahl, and H. Balakrishnan, “Glimpse: Continuous, real-time object recognition on mobile devices,” in *Proceedings of the 13th ACM conference on embedded networked sensor systems (SenSys)*, 2015, pp. 155–168.

[26] M. Caron, H. Touvron, I. Misra, H. Jégou, J. Mairal, P. Bojanowski, and A. Joulin, “Emerging properties in self-supervised vision transformers,” in *Proceedings of the IEEE/CVF international conference on computer vision (ICCV)*, 2021, pp. 9650–9660.

[27] K. He, X. Chen, S. Xie, Y. Li, P. Dollár, and R. Girshick, “Masked autoencoders are scalable vision learners,” in *Proceedings of the IEEE/CVF conference on computer vision and pattern recognition (CVPR)*, 2022, pp. 16 000–16 009.

[28] Y. Rao, W. Zhao, B. Liu, J. Lu, J. Zhou, and C.-J. Hsieh, “Dynamicvit: Efficient vision transformers with dynamic token sparsification,” in *Proceedings of the 35th Conference on Neural Information Processing Systems (NeurIPS)*, 2021, pp. 13 937–13 949.

[29] D. Bolya, C.-Y. Fu, X. Dai, P. Zhang, C. Feichtenhofer, and J. Hoffman, “Token merging: Your vit but faster,” in *The Eleventh International Conference on Learning Representations (ICLR)*, 2023.

[30] S. Long, Z. Zhao, J. Pi, S. Wang, and J. Wang, “Beyond attentive tokens: Incorporating token importance and diversity for efficient vision transformers,” in *Proceedings of the IEEE/CVF Conference on Computer Vision and Pattern Recognition (CVPR)*, 2023, pp. 10 334–10 343.

[31] C. Ryali, Y.-T. Hu, D. Bolya, C. Wei, H. Fan, P.-Y. Huang, V. Aggarwal, A. Chowdhury, O. Poursaeed, J. Hoffman *et al.*, “Hiera: A hierarchical vision transformer without the bells-and-whistles,” in *International Conference on Machine Learning (ICML)*. PMLR, 2023, pp. 29 441–29 454.

[32] M. Research, “Detectron2 - projects - vitdet,” <https://github.com/facebookresearch/detectron2/tree/main/projects/ViT-Det>, 2026, [Online; accessed 15-Jan-2026].

[33] OpenCV, “How to use background subtraction methods,” https://docs.opencv.org/4.x/d1/dc5/tutorial_background_subtraction.html, 2026, [Online; accessed 15-Jan-2026].

[34] J. Lee, S. Lee, J. Lee, S. Sathyaranayana, H. Lim, J. Lee, X. Zhu, S. Ramakrishnan, D. Grunwald, K. Lee *et al.*, “Perceive: Deep learning-based cellular uplink prediction using real-time scheduling patterns,” in *Proceedings of the 18th International Conference on Mobile Systems, Applications, and Services (MobiSys)*, 2020, pp. 377–390.

[35] A. Narayanan, E. Ramadan, R. Mehta, X. Hu, Q. Liu, R. A. Fezeu, U. K. Dayalan, S. Verma, P. Ji, T. Li *et al.*, “Lumos5g: Mapping and predicting commercial mmwave 5g throughput,” in *Proceedings of the ACM Internet Measurement Conference (IMC)*, 2020, pp. 176–193.

[36] G. Lv, Q. Wu, W. Wang, Z. Li, and G. Xie, “Lumos: Towards better video streaming qoe through accurate throughput prediction,” in *IEEE Conference on Computer Communications (INFOCOM)*. IEEE, 2022, pp. 650–659.

[37] K. Li, H. Nie, H. Gao, and X. Yao, “Knee point identification based on trade-off utility,” *arXiv preprint arXiv:2005.11600*, 2020.

[38] NVIDIA, “Jetson orin nano developer kit getting started guide,” <https://developer.nvidia.com/embedded/learn/get-started-jetson-orin-nano-devkit>, 2026, [Online; accessed 15-Jan-2026].

[39] R. Netravali, A. Sivaraman, S. Das, A. Goyal, K. Winstein, J. Mickens, and H. Balakrishnan, “Mahimahi: accurate {Record-and-Replay} for {HTTP},” in *2015 USENIX Annual Technical Conference (ATC)*, 2015, pp. 417–429.

[40] ZeroMQ, “An open-source universal messaging library,” <https://zeromq.org/>, 2026, [Online; accessed 15-Jan-2026].

- [41] OpenCV, “Opencv: Open source computer vision library,” <https://opencv.org/>, 2026, [Online; accessed 15-Jan-2026].
- [42] ———, “Vit tracker.” https://github.com/opencv/opencv_zoo/tree/main/models/object_tracking_vittrack, 2026, [Online; accessed 15-Jan-2026].
- [43] YouTube, “A walk down gold hill, shafesbury, english countryside 4k,” <https://www.youtube.com/watch?v=0gnm6gGMC3c>, 2026, [Online; accessed 15-Jan-2026].
- [44] ———, “Gentle rainfall walk in mexico city, binaural audio,” https://www.youtube.com/watch?v=h_FmnmBKZI, 2026, [Online; accessed 15-Jan-2026].
- [45] ———, “Cycling from brentwood to hollywood | 4k,” <https://www.youtube.com/watch?v=mjaHoNEuM-o>, 2026, [Online; accessed 15-Jan-2026].
- [46] ———, “Mexico city 4k - night drive,” <https://www.youtube.com/watch?v=oxZBX-e84O8>, 2026, [Online; accessed 15-Jan-2026].
- [47] Insta360, “Insta360 go 3s – the tiny mighty 4k cam,” <https://www.insta360.com/product/insta360-go3s>, 2026, [Online; accessed 15-Jan-2026].
- [48] Gstreamer, “Gstreamer: open source multimedia framework,” <https://gstreamer.freedesktop.org/>, 2026, [Online; accessed 15-Jan-2026].
- [49] M. Ghoshal, Z. J. Kong, Q. Xu, Z. Lu, S. Aggarwal, I. Khan, Y. Li, Y. C. Hu, and D. Koutsoukos, “An in-depth study of uplink performance of 5g mmwave networks,” in *Proceedings of the ACM SIGCOMM Workshop on 5G and Beyond Network Measurements, Modeling, and Use Cases*, 2022, pp. 29–35.
- [50] M. Ghoshal, I. Khan, Z. J. Kong, P. Dinh, J. Meng, Y. C. Hu, and D. Koutsoukos, “Performance of cellular networks on the wheels,” in *Proceedings of the 23rd ACM Internet Measurement Conference (IMC)*, 2023.
- [51] D. Raca, J. J. Quinlan, A. H. Zahran, and C. J. Sreenan, “Beyond throughput: A 4g lte dataset with channel and context metrics,” in *Proceedings of the 9th ACM multimedia systems conference (MMSys)*, 2018, pp. 460–465.
- [52] Optuna, “An open source hyperparameter optimization framework to automate hyperparameter search,” <https://optuna.org/>, 2026, [Online; accessed 15-Jan-2026].
- [53] P. Dash, Z. J. Kong, Y. C. Hu, C. Turner, D. Wolfensperger, M. G. Choi, A. Kshitij, and V. E. McLandrich, “How to pipeline frame transfer and server inference in edge-assisted ar to optimize ar task accuracy?” in *Proceedings of the 6th International Workshop on Edge Systems, Analytics and Networking (EdgeSys)*, 2023, pp. 36–41.
- [54] K. Du, A. Pervaiz, X. Yuan, A. Chowdhery, Q. Zhang, H. Hoffmann, and J. Jiang, “Server-driven video streaming for deep learning inference,” in *Proceedings of the Annual conference of the ACM Special Interest Group on Data Communication on the applications, technologies, architectures, and protocols for computer communication (SIGCOMM)*, 2020, pp. 557–570.
- [55] H. Mao, R. Netravali, and M. Alizadeh, “Neural adaptive video streaming with pensieve,” in *Proceedings of the 2017 Conference of the ACM Special Interest Group on Data Communication (SIGCOMM)*, 2017, pp. 197–210.
- [56] H. Fang, H. Zhao, J. Shi, M. Zhang, G. Wu, Y. C. Chou, F. Wang, and J. Liu, “Robust live streaming over leo satellite constellations: Measurement, analysis, and handover-aware adaptation,” in *Proceedings of the 32nd ACM International Conference on Multimedia (MM)*, 2024, pp. 5958–5966.
- [57] Y. Zhu, Y. Huang, X. Qiao, X. Liu, X. Su, A. Brunström, Ö. Alay, and S. Tarkoma, “Fpselector: A flexible path selector for mobile augmented reality offloading,” *IEEE Transactions on Mobile Computing (TMC)*, vol. 24, no. 9, pp. 8423–8440, 2025.
- [58] L. Jiang, S. D. Fu, Y. Zhu, and B. Li, “Janus: Collaborative vision transformer under dynamic network environment,” in *IEEE Conference on Computer Communications (INFOCOM)*. IEEE, 2025, pp. 1–10.
- [59] Y. Liu, R. Lu, and D. Wang, “Lvmscissor: Split and schedule large vision model inference on mobile edges via salp swarm algorithm,” *IEEE Transactions on Mobile Computing (TMC)*, vol. 24, no. 8, pp. 7538–7553, 2025.
- [60] S. Zhao, T. Liu, H. Jin, and D. Yao, “Spirit: Accelerate vision transformer inference on mobile devices via adaptive splitting and offloading,” *IEEE Transactions on Mobile Computing (TMC)*, vol. 24, no. 10, pp. 9303–9318, 2025.